

Synthesis, Modification, and Characterization of Fe₃O₄@SiO₂-PEI-Dextranase Nanoparticles for Enzymatic Degradation of Dextran in Fermented Mash

Authors:

Luis Pablo Amador-Gómez, Guadalupe Luna Solano, Galo Rafael Urrea-García, Ruby Sheila Gines-Palestino, Denis Cantú-Lozano

Date Submitted: 2023-02-17

Keywords: immobilization, dextranase, MNPs, dextran

Abstract:

During the sugar production process, undesirable compounds such as dextrans are produced and contaminate the flow of the sugar mill, reaching levels in the fluid of more than 10,000 ppm. Dextranase is an enzyme that has different industrial applications, since it catalyzes the hydrolysis of the bonds in random sites of the dextran. Therefore, the enzyme was immobilized using synthesized ferrite magnetic nanoparticles to degrade dextran in the fermented mash, because it is suitable to reuse and has a large surface area to bind dextranase on a solid carrier for easy magnetic separation. The synthesized bare and modified nanoparticles were characterized using SEM, EDS, FTIR, and XRD and confirmed the core-shell silica by increasing the silica composition from 0.2% of bare Fe₃O₄ NPs to 31.3% of modified Fe₃O₄ NPs. Ultrasonic treatment reduced the calculated crystal size with Scherer's equation from 91.3 to 13.5 nm, providing more particles for immobilization. The solvothermal process synthesized ferrite nanoparticles (Fe₃O₄) and modified them with TEOS and PEI. The obtained immobilization efficiency was 28%. Perhaps it was lower; Fe₃O₄ degraded almost the same as the free enzyme. The percentage of dextran degradation with free enzymes and immobilized enzymes with Fe₃O₄ magnetic nanoparticles was 61 and 52%, respectively.

Record Type: Published Article

Submitted To: LAPSE (Living Archive for Process Systems Engineering)

Citation (overall record, always the latest version):

LAPSE:2023.0106

Citation (this specific file, latest version):

LAPSE:2023.0106-1

Citation (this specific file, this version):


LAPSE:2023.0106-1v1

DOI of Published Version: <https://doi.org/10.3390/pr11010070>

License: Creative Commons Attribution 4.0 International (CC BY 4.0)

Article

Synthesis, Modification, and Characterization of $\text{Fe}_3\text{O}_4@\text{SiO}_2$ -PEI-Dextranase Nanoparticles for Enzymatic Degradation of Dextran in Fermented Mash

Luis Pablo Amador-Gómez , Guadalupe Luna Solano , Galo Rafael Urrea-García, Ruby Sheila Gines-Palestino and Denis Cantú-Lozano *

División de Estudios de Posgrado e Investigación, Tecnológico Nacional de México/Instituto Tecnológico de Orizaba, Av. Tecnológico No. 852 Col. E. Zapata, Orizaba 94320, Veracruz, Mexico

* Correspondence: denis.cl@orizaba.tecnm.mx; Tel.: +52-272-116-9456

Abstract: During the sugar production process, undesirable compounds such as dextrans are produced and contaminate the flow of the sugar mill, reaching levels in the fluid of more than 10,000 ppm. Dextranase is an enzyme that has different industrial applications, since it catalyzes the hydrolysis of the bonds in random sites of the dextran. Therefore, the enzyme was immobilized using synthesized ferrite magnetic nanoparticles to degrade dextran in the fermented mash, because it is suitable to reuse and has a large surface area to bind dextranase on a solid carrier for easy magnetic separation. The synthesized bare and modified nanoparticles were characterized using SEM, EDS, FTIR, and XRD and confirmed the core-shell silica by increasing the silica composition from 0.2% of bare Fe_3O_4 NPs to 31.3% of modified Fe_3O_4 NPs. Ultrasonic treatment reduced the calculated crystal size with Scherer's equation from 91.3 to 13.5 nm, providing more particles for immobilization. The solvothermal process synthesized ferrite nanoparticles (Fe_3O_4) and modified them with TEOS and PEI. The obtained immobilization efficiency was 28%. Perhaps it was lower; Fe_3O_4 degraded almost the same as the free enzyme. The percentage of dextran degradation with free enzymes and immobilized enzymes with Fe_3O_4 magnetic nanoparticles was 61 and 52%, respectively.

Keywords: immobilization; dextranase; MNPs; dextran



Citation: Amador-Gómez, L.P.; Luna Solano, G.; Urrea-García, G.R.; Gines-Palestino, R.S.; Cantú-Lozano, D. Synthesis, Modification, and Characterization of $\text{Fe}_3\text{O}_4@\text{SiO}_2$ -PEI-Dextranase Nanoparticles for Enzymatic Degradation of Dextran in Fermented Mash. *Processes* **2023**, *11*, 70. <https://doi.org/10.3390/pr11010070>

Academic Editors: M. Ali Aboudzadeh and Shaghayegh Hamzehlou

Received: 8 November 2022

Revised: 22 December 2022

Accepted: 23 December 2022

Published: 27 December 2022



Copyright: © 2022 by the authors. Licensee MDPI, Basel, Switzerland. This article is an open access article distributed under the terms and conditions of the Creative Commons Attribution (CC BY) license (<https://creativecommons.org/licenses/by/4.0/>).

1. Introduction

During the sugar production process, dextrans are undesirable compounds produced by *Leuconostoc mesenteroides*, which can quickly utilize high percentages of presented sugar in juices. Under favorable temperature and humidity conditions, dextransucrase hydrolyses sucrose forms dextrans [1]. Dextrans are extracted in mills and juices. They contaminate sugar mill flow, producing levels in the fluid exceeding 10,000 ppm (1%) in extreme cases. In burnt sugar cane, a rapid increase in the level of dextrans of almost ten times was observed from 12 to 48 h, reaching 3200 ppm [2,3].

Dextran is a neutral and branched naturally occurring polysaccharide composed of a main linear chain of α -1,6 glycosidic linkages with a few branches of α -glucopyranose at positions (0-2), (0-3) or (0-4) [4,5]. Dextran is a biodegradable polymer synthesized by lactic acid bacteria, mainly belonging to the *Leuconostoc* genera [6,7].

Dextran degradation entails several glycosyl hydrolases with different specificities and modes of action. These enzymes are called endo- and exodextranases. Dextranase (1,6- α -D-glucan-6-glucanohydrolase) is an enzyme that catalyzes the hydrolysis of α -(1-6)-d-glycoside linkages in random sites of dextran [8].

Dextranases have important industrial applications, since these enzymes can depolymerize various troublesome microbial dextran deposits [9] and catalyze the degradation of dextran into low-molecular weight fractions [1,5]. Free enzymes in solution are more sensitive to environmental changes compared to immobilized enzymes. Immobilization

techniques have high potential both industrially and scientifically due to their economic and technological importance [10].

The development of dextranase-immobilization technology is expected to provide a promising technology for dextran's reuse. The purpose of immobilization is to immobilize an enzyme inside or on the surface of an insoluble material such that the enzyme's catalytic activity is maintained, allowing the easy recovery of the enzyme, rapid termination of the enzyme assay, and repeated enzyme assay, which will reduce the assay cost. In addition, after immobilization, the storage stability, pH, and thermal resistance are usually improved [11,12]. Based on these advantages, immobilized enzymes have been widely applied in various fields such as the pharmaceutical industry, the food industry, wastewater treatment, and the textile industry [11]. Immobilization strategies generally focus on continuous operation, increasing stability, and reducing the usage of enzymes. The feasibility of immobilizing dextranase on different support materials has been verified via physical adsorption, ion adsorption, encapsulation, and covalent adsorption. However, it remains a challenge to identify materials that provide the requirements of special characteristics for higher enzyme immobilization efficiency. Moreover, the robustness and costs of immobilization are significant factors that affect the applications of immobilization. Ideally, the carrier material should have a relatively high specific surface area to enable the immobilization of a large amount of enzyme. Moreover, hydrophilicity with good infusibility and low substrate solubility could avoid product contamination. From the immobilization of biocatalysts to the recovery of enzymes, the mechanical resistance and thermal stability of the scaffolds are important throughout the process [5].

Magnetic nanoparticles (MNPs) are one of the most promising nanomaterials in various biomedical applications. MNPs are widely synthesized by thermal decomposition in high-boiling point organic solvents to give hydrophobic particles or, by co-precipitation in an aqueous media, to give water-dispersible ones. The advantage of the former method is that it can offer excellent control over the particle size, shape, and uniformity [13,14]. However, the resulting hydrophobic particles must be surface modified to make them water dispersible before any biomedical applications; for example, another type of lipid-polymer hybrid nanoparticle has been used to enhance the solubility and bioavailability of poorly soluble drugs, as well as the permeability of bioactive compounds [15]. On the other hand, MNPs synthesized by the latter method typically show broader size distributions, but the resulting MNPs are often water dispersible and compatible with most biomedical applications. Among the many different types of MNPs, iron oxide-based nanoparticles, such as magnetite (Fe_3O_4) and maghemite ($\gamma\text{-Fe}_2\text{O}_3$), have attracted significant interest in broad biomedical and diagnostic areas because of their low-/non-toxicity and excellent biocompatibility [16,17].

Among several MNPs such as iron oxide-based (Fe_3O_4 and $\gamma\text{-Fe}_2\text{O}_3$), pure metal-based (Fe and Co), spinel-type ferromagnet-based (MgFe_2O_4 , MnFe_2O_4 , and CoFe_2O_4), and alloy-based (CoPt_3 and Fe-Pt) MNPs, Fe_3O_4 NPs are the most frequently used for enzyme immobilization due to their superior advantages of non-toxicity and good biocompatibility. Magnetic nanoparticles made of iron, cobalt, or nickel oxides exhibit special properties, including a high surface-to-volume ratio and high magnetic moment, allowing potential manipulation by an external magnetic field. Especially manufactured MNPs with a ferromagnetic material, i.e., iron oxide nanoparticles (IONPs) made of magnetite (Fe_3O_4) and maghemite ($\gamma\text{-Fe}_3\text{O}_4$), combine ideal biocompatibility with superparamagnetic properties [18]. Many synthetic methods have been developed for synthesizing Fe_3O_4 NPs, including chemical co-precipitation, microemulsion, thermal decomposition, and solvothermal synthesis [19]. The solvothermal method is useful for the synthesis of ferrite materials with improved physical and chemical properties applicable to both industrial and biomedical areas. In the solvothermal synthesis method, aqueous or nonaqueous solvents can be used to synthesize ferrite materials with precise control over the size distribution, shape, and crystalline phases. The physical characteristics can be altered by changing

certain experimental parameters, such as the reaction temperature, reaction time, solvent, surfactant, and precursors [20].

Fe₃O₄ NPs tend to aggregate because of their high surface energy caused by the large specific surface area. Moreover, Fe₃O₄ NPs possess high chemical activity and are easily oxidized in air, resulting in loss of magnetism and dispersibility. These factors could make the magnetic separation less effective. Hence, the naked Fe₃O₄ NPs cannot be used directly for enzyme immobilization. The surface modification is favorable for preventing the aggregation and oxidation of Fe₃O₄ NPs used as support matrices for enzyme immobilization [12,13,16,21]. Fe₃O₄ NPs have limitations, such as rapid agglomeration, wide surface area, high chemical reactivity, and high surface energy, resulting in magnetism loss. Therefore, appropriate surface modification of Fe₃O₄ NPs is required to avoid the abovementioned problems. The coating is the most common surface modification method to conjugate organic or inorganic materials onto the surface of iron oxide nanoparticles. This approach avoids oxidation and agglomeration and provides the possibility of further functionalization. The functionalization of magnetic NPs boosts their physicochemical properties, making them ideal candidates for catalysis [22].

Silica coating is a typical method for modifying Fe₃O₄ NPs, in which silica shells form on the surfaces of magnetic cores. The silica shells protect the magnetic cores from aggregation and oxidization, thus improving chemical stability. Moreover, silica shells can also improve hydrophilicity and biocompatibility. After modification, substantial silanol groups are introduced on the surfaces of magnetic cores, which will provide the underlying basis for further improvement with functional reagents for enzyme immobilization. There are two modes for modifying MNPs with organic polymers, the *in situ* modification mode and the *ex situ* modification mode. The steric repulsion generated from polymer coatings will weaken the magnetic forces and van der Waals forces of Fe₃O₄ NPs, thus preventing their aggregation and improving their dispersibility and stability. Owing to excellent biocompatibility and biodegradability to amino polymers such as chitosan, polyethyleneimine (PEI), and polydopamine, they are usually used to modify Fe₃O₄ NPs for enzyme immobilization [12,13].

On the other hand, when enzyme proteins are directly immobilized on the surface of magnetic particles, the loading capacities are limited because of the existence of steric hindrance between the carrier surface and the immobilized enzyme protein. Among the spacer-arm molecules, high-molecular weight biopolymers, such as polyethylenimine (PEI), display distinct advantages. The long and flexible chains of PEI polymer decrease steric hindrance and provide abundant function amino groups for immobilizing enzyme proteins and preventing particle agglomeration [23]. Due to the above, it is important to highlight the importance of polymer modification or hybridization to improve performance in different processes; for example, graphene and carbon nanotubes' nanoparticles were used as a radical-scavenging filler for capture and quench free radicals in a UV-protective waterborne polymer coating [24].

In addition, several reactors have been used to immobilize enzymes such as OTC-IMER, MC-IMER, and capillary columns [12,25]. On the other hand, rotary disk reactors have been used for degradation because of their easy handling and low-cost energy consumption [26].

This research aims to immobilize dextranase with Fe₃O₄ MNPs as a scaffold for dextran degradation contained in the fermented mash; these immobilized enzymes would allow easy and rapid recovery. On the other hand, the solvothermal process would help to control crystal size and shape. After that, they are modified with the silica shell to avoid agglomeration and oxidation to improve enzyme recovery and the degradation process compared with the free enzyme.

2. Materials and Methods

2.1. Chemical Materials and Reagents

Dextran T100 (100KDa), branched polyethyleneimine (25,000 average molecular weight), tetraethyl orthosilicate (TEOS, 99%), (3-aminopropyl) triethoxysilane (APTS 99%), glutaraldehyde (50%), bovine seroalbumin (BSA, 98%), sodium borohydride (NaBH_4), ethylene glycol anhydrous (99.8%), polyethylene glycol (200 average molecular weight), and 3,5-dinitrosalicylic acid (98%) were purchased from the Sigma-Aldrich brand. Ammonia solution ($\text{NH}_3\text{H}_2\text{O}$, 28% *w/v*), cupric sulfate pentahydrate (ACS), anhydrous sodium carbonate (ACS), sodium potassium tartrate, 4-hydrated (ACS), Sodium sulfate anhydrous (ACS), sodium citrate dihydrate (ACS), phenol (ACS), glacial acetic acid, and diatomaceous earth were obtained from J.T BAKER. Sodium hydroxide (ACS), sodium acetate (ACS), dibasic sodium phosphate heptahydrate (ACS), monobasic sodium phosphate (ACS), sodium sulfite (ACS), sulfuric acid 98–99% (ACS), potassium dichromate (ACS), mercuric sulfate (ACS), silver sulfate (ACS), and potassium biphthalate (ACS) were obtained from Fermont. Phenol Folin–Ciocalteu reagent was obtained from HYCEL, absolute ethyl alcohol was obtained from Karol, and isopropyl alcohol (ACS) was obtained from Mallinckrodt.

2.2. Sugarcane Mash Obtainment

Sugarcane mash was obtained from a local bioethanol-producing company in Orizaba, Veracruz, Mexico, which receives molasses from different regional sugar mills.

2.3. Characterization of Fermented Sugarcane Mash

The pH was determined with a Hanna Instruments Model HI2211 potentiometer. The density was calculated by pycnometer, the moisture content was calculated by gravimetry, the sucrose content (°Brix) was determined with a refractometer, and the reducing sugars were determined with the Miller Technique (3,5-dinitrosalicylic acid method) using a 1 mg/mL maltose solution as a standard. Total carbohydrates were determined by the Antrona-Sulfuric technique, the amount of protein was quantified by the Lowry technique, and the dextran concentration was determined by AOAC988 (Robert's copper method) using standard dextran from *Leuconostoc* Spp. Mr100000 at 20 g/L. Total and volatile suspended solids were determined with SM 2540D and 2540E, respectively, as well as total and soluble chemical oxygen demand with SM 5220D. All experiments were performed in triplicate. Rheological characterization and calculation of the viscosity of the fermented mash was carried out on an Anton Paar Model MCR301 rheometer and Rheoplus/32 V2.81 software for data capture and analysis. A cylinder Peltier (C-PTD200-SN80123149) and stirrer geometry (ST22-4V-40-SN10120) were used for fermented sugar cane mash over a wide shear rate range of 0 to 1000 1/s at 25 °C.

2.4. Obtaining the Enzyme

Commercial endodextranase Plurizyme DEX 96 from a fungal strain *Chaetomium* spp. was purchased from the company PLURICHEM in Córdoba, Veracruz, México.

2.5. Characterization of the Enzyme

2.5.1. Rheological Characterization of Commercial Enzyme

Rheological characterization was performed on an Anton Paar Model MCR301 rheometer and Rheoplus/32 V2.81 software for data capture and analysis. A cylinder Peltier (C-PTD200-SN80123149) and stirrer geometry (ST22-4V-40-SN10120) were used over a wide shear rate range of 0 to 1000 1/s at 25 °C.

2.5.2. Determination of Dextranase Activity

The enzymatic activity of the free enzyme was determined using dextran (Mr100000). An amount of 0.4 mL of the free enzyme was suspended in 1.6 mL of acetate buffer solution (0.1 M, pH 5.5) containing dextran (20 g/L) and then heated at 55 °C for 15 min. The determination of reducing sugars was carried out by Miller's technique (3,5-dinitrosalicylic

acid method) using a VELAB Model: VE-5100UV UV-VIS spectrophotometer at 540 nm. One unit (U) of dextranase activity was defined as the enzyme needed to catalyze the liberation of 1 μmol of maltose per minute from dextran (Mr100000).

2.5.3. Determination of pH Stability Determination

The pH stability was determined by mixing 2 mL of the free enzyme with 10 mL of 0.1 M acetate buffer solution containing dextran (20 g/L) ranging in pH from 3.5 to 5.5 and 0.1 M phosphate buffer solution from pH 6 to 6.5, then heating at 55 °C for 15 min. The determination of reducing sugars was carried out by Miller's technique (3,5-dinitrosalicylic acid method) in each buffer solution using a VELAB model: VE-5100UV UV-VIS spectrophotometer at 540 nm. One unit (U) of dextranase activity was defined as the enzyme needed to catalyze the liberation of 1 μmol of maltose per minute from dextran (Mr100000).

2.5.4. Determination of pH Stability Determination

The temperature stability was determined by adding 2 mL of the free enzyme with 10 mL of 0.1 M acetate buffer solution at pH 5.5 containing dextran (20 g/L). Then, this procedure was engaged from 30 to 70 °C, at the end of which the enzyme activity was calculated. One unit (U) of dextranase activity was defined as the enzyme needed to catalyze the liberation of 1 μmol of maltose per minute from dextran (Mr100000).

2.6. Synthesis of Magnetite Nanoparticles (Fe-NPs) and Modification with TEOS and PEI ($\text{Fe}_3\text{O}_4@\text{SiO}_2\text{-PEI}$)

Synthesis of the magnetite nanoparticles was carried out with the solvothermal process [23,27] with several technical modifications. Iron chloride III hexahydrate was used ($\text{FeCl}_3\cdot 6\text{H}_2\text{O}$) as a precursor and source of iron, ethylene glycol 99.8% ($\text{HOCH}_2\text{CH}_2\text{OH}$) as a solvent, polyethylene glycol Mw:200 ($\text{H}(\text{OCH}_2\text{CH}_2)_n\text{OH}$) as a surfactant, along with anhydrous sodium carbonate (Na_2CO_3). The mixture was placed in a Teflon-lined stainless-steel autoclave reactor (100 mL capacity) to be stirred at 238 rpm for 30 min. The autoclave was heated in a muffle at 195 °C (± 5) for eight hours, then allowed to cool to room temperature for approximately 15 h. Magnetic separation and decantation were carried out using a micropipette to separate the supernatant and thus ensure that the products were not sucked out. Five washes were made with 5 mL of ethanol and distilled water, separating with a magnet in each wash. The product was dried at 60 °C for 6 h in an oven. One gram of nanoparticles was weighed and dispersed in a solution of 200 mL of distilled water, 800 mL of ethanol, and 6 mL of 28% ammonium solution ($\text{NH}_3\text{H}_2\text{O}$), which were taken to ultrasound treatment in a Cole-Parmer 500-Watt processor for 30 min at 40% amplitude to break down the particle agglomerates and improve the functionalization surface. Subsequently, 6 mL of tetraethylortosilicate was added (TEOS) to 30 °C for 12 h with constant agitation of 238 rpm. After the reaction time, the supernatant was separated; three washes of 50 mL of water, ethanol, and isopropanol were carried out with magnetic separation in each wash. The washed particles were suspended in 400 mL of isopropanol with the addition of 2 mL of aminopropyltriethoxysilane (APTS) in constant agitation (525 rpm) at 30 °C for 24 h for subsequent immobilization.

2.7. Characterization of Bare Fe-NPs and Modified Fe-NPs

Surface morphology was observed by high-resolution SEM (XL30-SFEG Philips/FEI brand) and inspected at an accelerating voltage of 20 kV an X-Max energy dispersive spectroscopy (EDS). An X-ray detector was used to obtain the elemental analysis, and the results were analyzed in ImageJ software to determine the morphology and the approximate diameter of the nanoparticles. Compositional characterization was analyzed by a Fourier-transform infrared spectrometer (FTIR) equipped with Agilent Cary 660 attenuated total reflectance (ATR) in the range of 4000 to 400 cm^{-1} . The structural analyses were carried out with XRD using a Siemens D5000 diffractometer with Siemens Diffract-AT software,

version 1 (Cu K α radiation $\lambda = 0.15406$ nm) in the Bragg–Brentano configuration. The diffractograms were analyzed in Match! 3.3 for crystal size determination and comparison with the standard.

The Scherrer formula was used to determine the crystal size (D) using Equation (1):

$$D = \frac{\beta_{hkl}}{4 \tan \theta} \quad (1)$$

where: D (nm)= crystal size, K(-)= form factor 0.9, λ (nm) = wavelength of X-ray radiation Cu K α ($\lambda = 0.15418$ nm), β = maximum intensity of half of the full width (FWHM), and θ = Bragg's angle.

For dislocation density, Equation (2) was used for (δ), which is directly related to strain and crystal size. Equation (3) was used to evaluate the material stress (ϵ) [28]:

$$(\delta) = \frac{1}{D^2} \quad (2)$$

$$(D) = \frac{\beta_{hkl}}{4 \tan \theta} \quad (3)$$

where: β = maximum intensity of half of the full width (FWHM), and θ = Bragg's angle.

2.8. Immobilization of Modified Fe₃O₄ NPs (Fe₃O₄@SiO₂-PEI-Dextranase)

Hereafter, magnetic separation of NPs was achieved with a magnet; three washes of 15 mL pour of distilled water were performed in a washed house and magnetically separated. Finally, the NPs were taken to an oven at 60° for 6 h. Subsequently, 40 mg of NPs were added from the dried product to a 100 mL phosphate buffer (0.1 M, pH 6.0) containing 5% (*w/v*) glutaraldehyde, which was brought to constant agitation at 350 rpm and 30 °C for 4 h. They were magnetically separated and washed three times with 10 mL of phosphate buffer (0.1 M, pH 6.0) to remove excess residual glutaraldehyde. The washed product was dispersed in 8 mL phosphate buffer (0.1 M, pH 6.0) containing 3.6118 mL of the enzyme (3.4748 mg protein/mL) and 0.0023 g of NaBH₄ (0.2 mg/mL) for subsequent agitation at 350 rpm and 30 °C for 4 h. At the end of the time, the supernatant was collected to determine the amount of residual protein and calculate the immobilization efficiency percentage. Four 1 mL washes were performed with phosphate buffer (0.1 M, pH 6.0) to remove non-covalently bound proteins; the wash solution was collected for protein quantification. Immobilized enzymes were suspended in acetate buffer (0.1 M, pH 5.5) and stored at 4 °C for later use [23].

Calculation of the immobilization efficiency was performed according to Equation (4):

$$\text{Immobilization efficiency [\%]} = 100 - \left[\left(\frac{\text{Nonbound protein}}{\text{Initial protein content}} \right) \times 100 \right] \quad (4)$$

The enzyme-carrying capacity in the nanoparticles was determined as described in Equation (5):

$$\text{Loading capacity} = \left(\frac{\text{Bound protein}}{\text{NPs initial weight}} \right) \quad (5)$$

2.9. Enzymatic Degradation of Dextran in Fermented Mash

In order to degrade the dextran contained in sugarcane fermented mash, enzymatic hydrolysis was carried out using the free and immobilized enzyme (Fe₃O₄@SiO₂-PEI-Dextranase) to make a comparison of performance degradation percentage; experiments were performed in triplicate. Fermented mash was used as a substrate; in a 250 mL flask, 100 mL of the substrate was added; for degradation experiments with the free enzyme, 1 mL of the enzyme was added to the flask and then put in a constant agitation of 250 rpm and heated to 55 °C for 1 and 2 h. For the degradation experiments of the immobilized enzyme, 1 mL of immobilized enzyme was used with the same conditions as before.

3. Results and Discussion

3.1. Physicochemical and Rheological Characterization of Fermented Sugarcane Mash

Physicochemical and rheological characterization of the fermented sugarcane mash was made according to point 2.5, shown in the methodology section. The characterization of the fermented mash in Table 1 was carried out; the fermented mash conforms to the Herschel–Bulkley model, presenting a dilating behavior demonstrated with the value of n : 1.8854 in Table 1. Fermented mash behaved as a dilatant fluid, showing a flow behavior greater than one ($n > 1$) Figure 1. This obtained behavior was the same as that from other authors who studied the same substrate [29]. Solid concentration decreased due to the alcohol production from sucrose [3].

Table 1. Herschel–Bulkley experimental model parameters for fermented mash at 25 °C.

Model	Experimental Model	R ²
Herschel–Bulkley	$\sigma = 0.0975 + 8.381 \times 10^{-5} \dot{\gamma}^{1.8854}$	0.9974

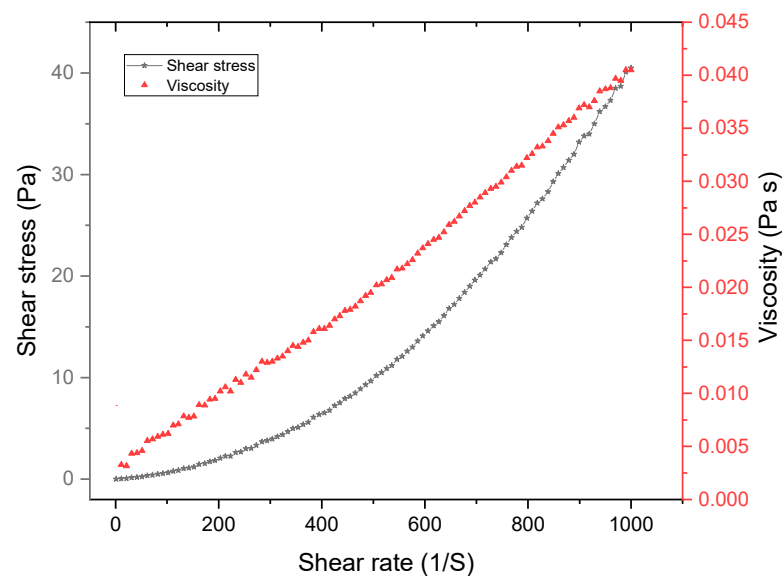


Figure 1. Rheological behavior of fermented mash at 25 °C.

In the characterization of the fermented mash in Table 2, each determination was performed in triplicate, showing a high concentration of dextrans and carbohydrates [30]. The mash had 75% fermentable sugars according to the ratio of reducing sugars/carbohydrates; even though it had 13° Brix, a rapid sucrose determination, this residue is suitable for an enzymatic treatment because of the determination of reducing sugars and total carbohydrates. Furthermore, the pH value of 5.21 is adequate for enzymatic degradation, and the dextran content of 1899.2 ppm is almost six times higher than other authors have found [3]. The protein concentration was determined because of the remaining yeast used for the bioethanol obtention process. According to TSS, TVS, TCOD, and SCOD, sugarcane-fermented mash has a high residual concentration of organic matter.

3.2. Characterization of the Enzyme

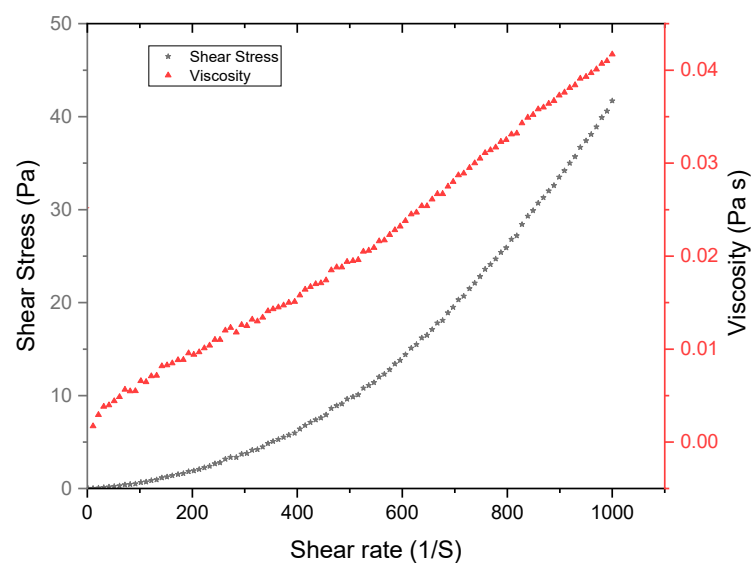
The free enzyme was rheologically characterized in Table 3, which conformed to the Herschel–Bulkley model and presented a dilating behavior (Figure 2) demonstrated by the value of n : 1.9181.

Table 2. Physicochemical characterization of fermented mash.

Determination	Value	Technique
pH	5.21 ± 0.11	Potentiometry
Density (g/mL)	1.02 ± 0.03	Pycnometry
Viscosity (Pa s)	0.02 ± 0.004	Rheometry
Moisture (%)	91.50 ± 1.8	Gravimetry
Brix (°)	13 ± 0.2	Refractometry
Reducing sugars (g/L)	22.23 ± 1.12	Miller DNS
Carbohydrates (g/L)	29.58 ± 2.46	Anthrone method
Dextran (ppm)	1899.20 ± 17.10	AOAC official method Dextran in raw cane sugar; Robert's copper method
Protein (mg/L)	0.40 ± 0.08	Lowry's method
Total suspended solids (TSS) (g/L)	16.40 ± 1.75	2540 D Standard methods
Total volatile solids (TVS) (g/L)	15.20 ± 2.54	2540 E Standard methods
Total chemical oxygen demand (TCOD) (g/L)	184.67 ± 12.43	5220 D Standard methods
Soluble chemical oxygen demand (SCOD) (g/L)	182.50 ± 8.85	5220 D Standard methods

Table 3. Herschel–Bulkley experimental model parameters for the enzyme at 25 °C.

Model	Experimental Model	R ²
Herschel–Bulkley	$\sigma = 0.0978 + 6.570 \times 10^{-5} \dot{\gamma}^{1.9181}$	0.9947

**Figure 2.** Rheological behavior of free dextranase at 25 °C.

Commercial dextranase comes from the fungal strain *Chaetomium* Spp. The calculated protein concentration was 0.9620 mg/mL, the enzymatic activity was 0.55 U/mL, and the higher enzymatic specific activity was 0.75 U/mg enzyme at 55 °C and 5.5 pH. Similar pH conditions were obtained by [31], the authors of which purified and isolated 12 strains of enzymes and obtained a maximum activity of 120 U/mL against 0.55 U/mL shown in Figure 3; we could say that this difference could be because of the origin of the enzyme and also the different methodology to calculate enzyme activity. Further, we could see differences in these parameters according to the immobilization method and dextranase strain used [32].

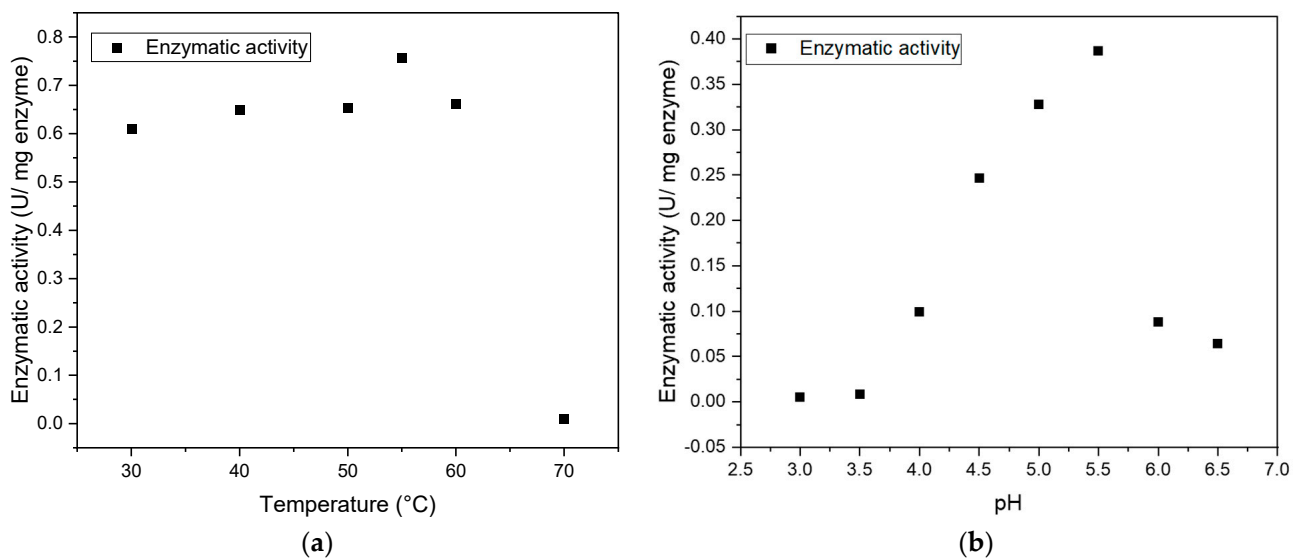


Figure 3. Enzymatic activity of free dextranase (a) at different temperatures and (b) at different pH.

3.3. Characterization of Magnetite Nanoparticles (SEM, EDS, XRD y FTIR)

3.3.1. Characterization of Bare Fe_3O_4 NPs

Figure 4 shows the SEM micrographs of synthesized nanoparticles. The synthesized MNPs obtained via the solvothermal process had an undetermined shape, possibly because Fe_3O_4 NPs tend to agglomerate [33].

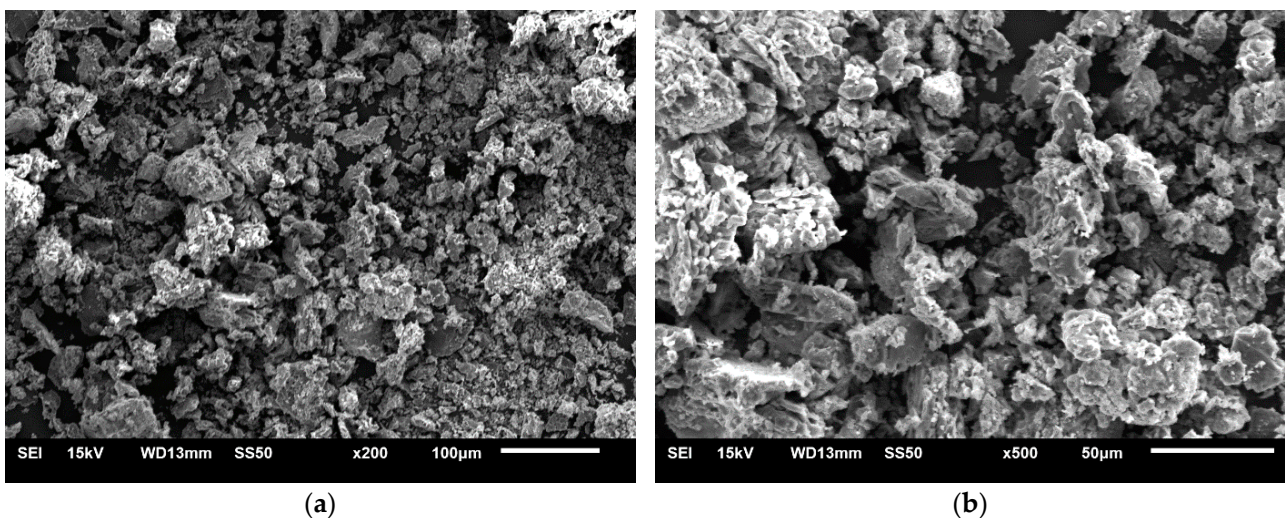


Figure 4. SEM micrographics of bare ferrite magnetic NPs: (a) 200 times, (b) 500 times.

EDS analysis of bare Fe_3O_4 shown in Figure 5 demonstrates the chemical composition and the percentage of some elements, such as 35.1% oxygen (O), 35.1% sodium (Na), 19.4% carbon (C), and 19.1% iron (Fe), in the body of the synthesized composite [22]. Further, some trace elements were identified, such as 1.4% chlorine (Cl), 0.5% copper (Cu), and 0.2% silica (Si).

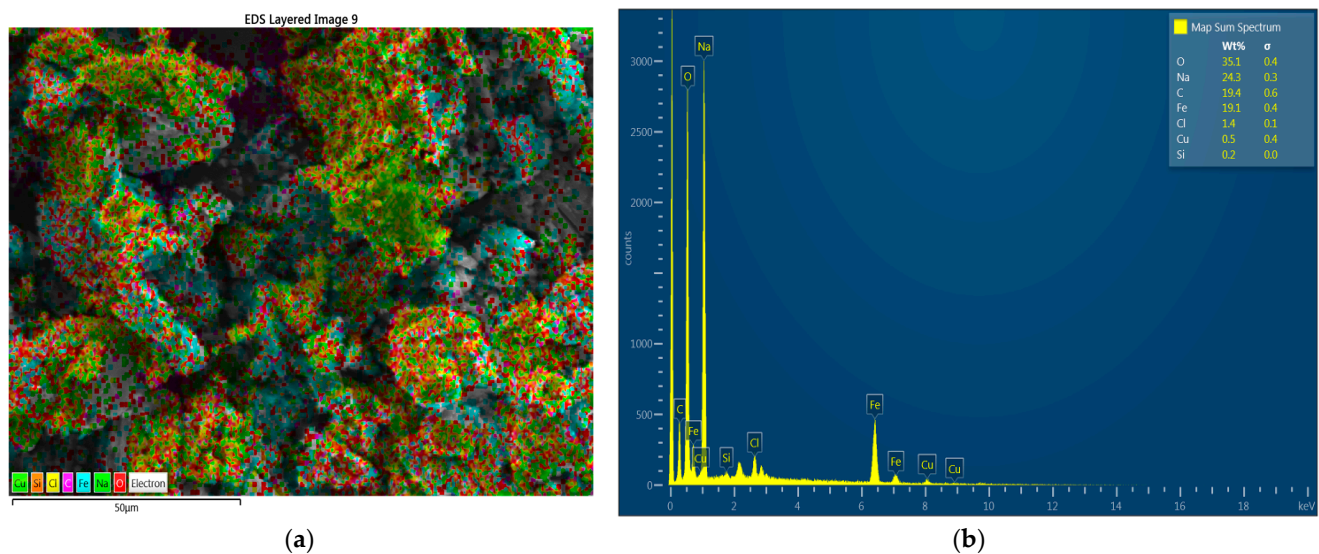


Figure 5. EDS image of bare Fe_3O_4 NPs: (a) EDS colorization layer of identified elements in SEM micrograph of bare Fe_3O_4 NPs, (b) EDS spectrum of bare Fe_3O_4 NPs containing O, Na, C, Fe, Cl, Cu, and Si.

X-ray diffractograms of bare Fe_3O_4 NPs are shown in Figure 6. The characteristic peaks at $2\theta = 45.41^\circ$, 66.21° , and 83.94° were assigned to reflections at (1 0 0), (2 0 0), and (2 1 1) indices based on the plane of the cubic spinel structure of Fe_3O_4 -MNPs; the obtained peaks correspond to the database (COD-Inorg REV140301) and are similar to those reported by [34,35]. With Match, these reflection points (Miller indices) were obtained, and the composition of iron present in the nanoparticle sample was identified [35].

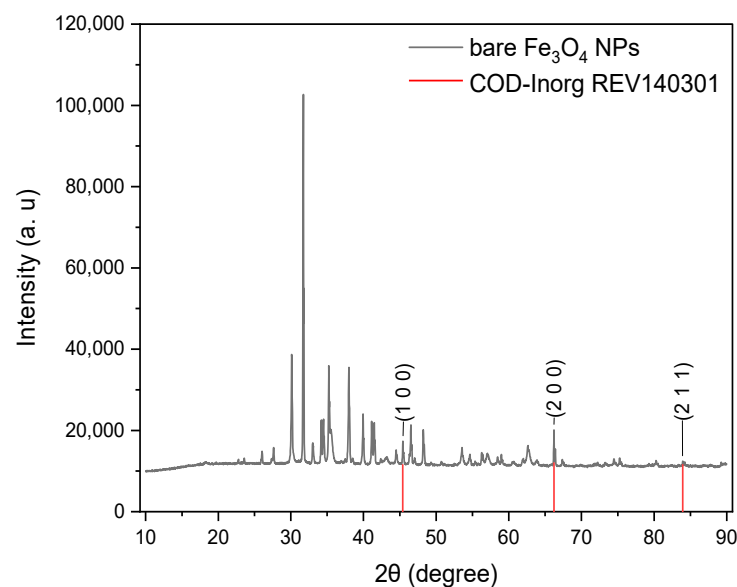


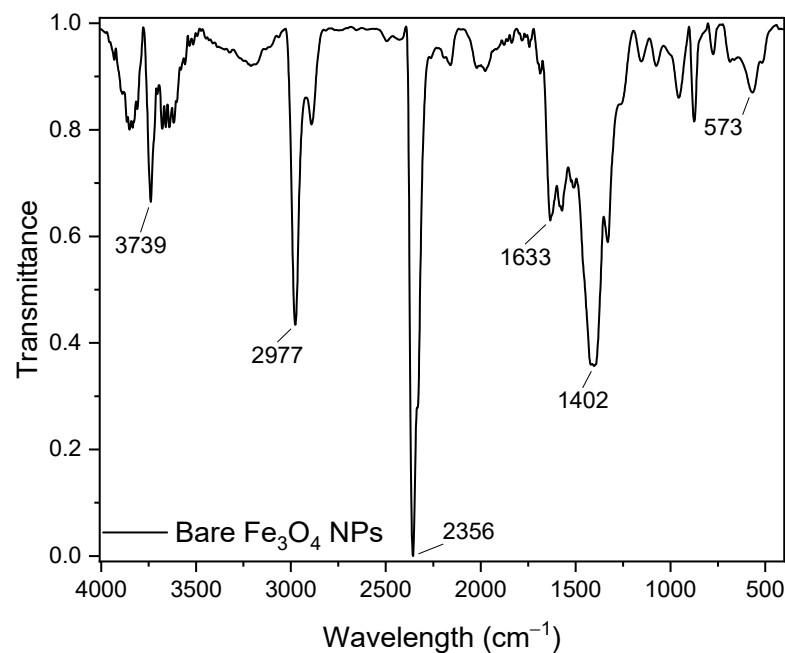
Figure 6. XRD patterns of bare Fe_3O_4 NPs.

In addition, FWHM values were obtained with Match! 3.3. Furthermore, with the Scherrer equation, the obtained average crystal size of the Fe_3O_4 -NPs was 91.36 ± 9.91 nm, as shown in Table 4, which is ten times greater than the results in [34,35], which can be attributed to the solvothermal process that could synthesize nanoparticles from 200 nm and greater depending on treatment time.

Table 4. Calculated crystallographic parameters of bare Fe₃O₄ NPs with data obtained from XRD analysis using the Scherrer equation.

2θ (Degree)	(hkl)	θ (Radian)	FWHM (Degree)	FWHM β(Radian)	Crystal Size D (nm)	Dislocation Density δ	Stress ε	Average Crystal Size D (nm)	Crystal Size De- viation D (nm)
45.41	(1 0 0)	0.3963	0.105	0.0018	82.0158	0.000149	0.00109	91.3666	9.9147
66.21	(2 0 0)	0.5778	0.105	0.0018	90.3217	0.000123	0.00070		
83.94	(2 1 1)	0.7325	0.105	0.0018	101.7625	0.000097	0.00051		

The infrared pattern of bare Fe₃O₄ is shown in Figure 7. The peak at 573 cm^{−1} corresponds to the tetrahedral and octahedral positions of iron; in other works in which nanoparticles of Fe₃O₄ were sintered, similar wavelengths 611, 548, 576, and 567 cm^{−1} were obtained, respectively [36–39]. On the other hand, the peak obtained at 1633 cm^{−1} corresponds to the bending vibrations of the water absorbed on the surface of iron oxide [36,38] obtained at a characteristic peak of 1620 cm^{−1}, which is close to the first peak obtained; the variation can be attributed to the fact that these are different processes of obtaining nanoparticles. Finally, the peak at 2356 cm^{−1} is close to that obtained by [38] at 2354 cm^{−1}, which was probably formed by the C-H stretching vibrations of impurities that did not react. The presence of this compound in the product obtained from the synthesis can be corroborated.

**Figure 7.** FTIR patterns of bare Fe₃O₄ NPs.

3.3.2. Characterization of Modified Fe₃O₄ NPs

The morphology of modified Fe₃O₄ NPs with TEOS was analyzed to corroborate the morphology as shown in Figure 8; the expected form according to the methodology is spherical, and their estimated size with ImageJ software in Figure 8a,b is observed with an average of 970 nm ± 120. In another work, the authors obtained a size of the modified particles of 230 nm [23].

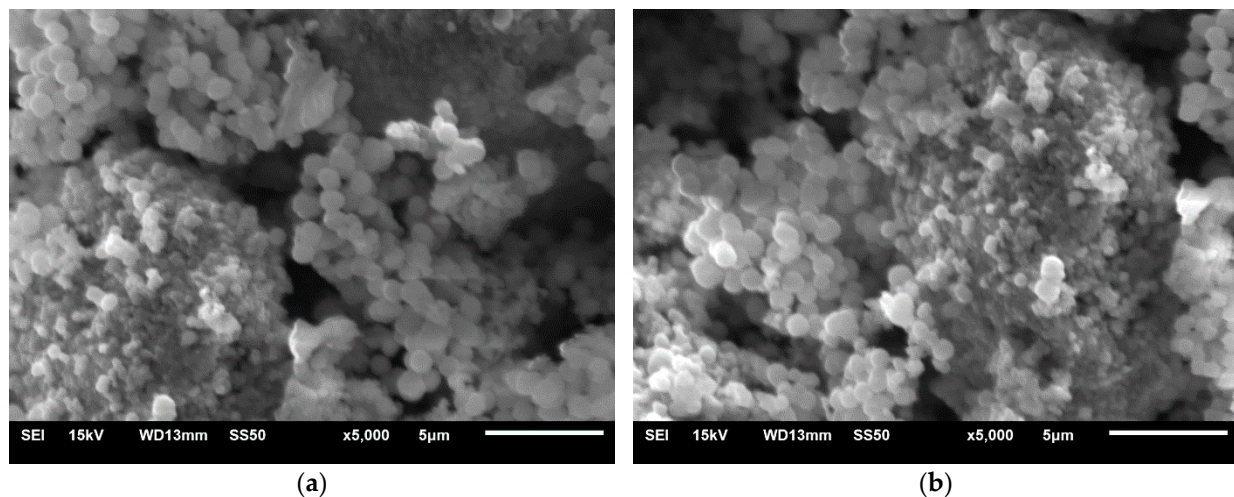


Figure 8. SEM micrographics of modified SEM Fe_3O_4 NPs: (a) 5000 times, (b) 5000 times.

EDS analysis coupled with SEM in Figure 9 was performed to demonstrate the chemical composition of modified nanoparticles and make a quantitative estimate composition of the sample. The silica composition increased from 0.2% in bare Fe_3O_4 NPs to 31.3% in modified Fe_3O_4 , and the Fe concentration decreased from 19.1% to 8.9%. This shows a wide silica shell formation on the surface of the Fe_3O_4 NPs [22], confirming that the modification process was accomplished.

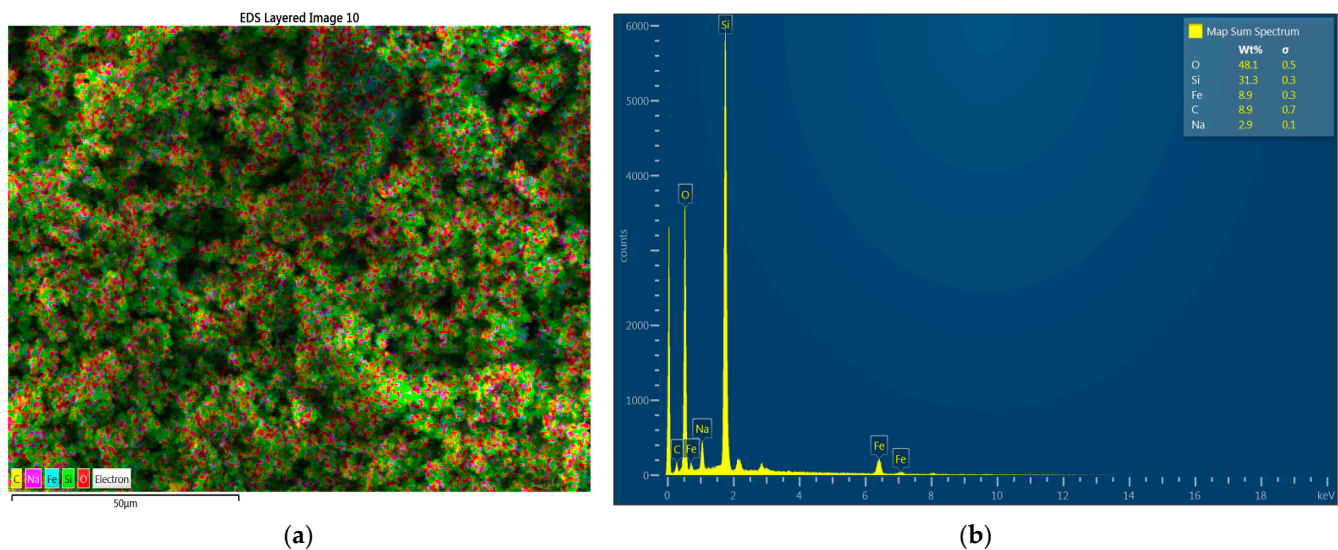


Figure 9. EDS image of modified Fe_3O_4 NPs: (a) EDS colorization layer of identified elements in a SEM micrograph of modified Fe_3O_4 NPs, (b) EDS spectrum of modified Fe_3O_4 NPs containing O, Si, Fe, C, Na.

The X-ray diffraction patterns of modified Fe_3O_4 are shown in Figure 10. The characteristic peaks at $2\theta = 18.43^\circ$, 30.19° , 35.55° , 43.22° , 57.16° , and 62.78° were assigned to reflections (1 1 1), (2 0 2), (3 1 1), (4 0 0), (5 1 1), and (4 0 4), respectively, which are similar to those reported by [34,35]. Further, these reflections indicate the plane of the cubic spinel structure of the Fe_3O_4 NPs [33]. It is worth mentioning that the modified nanoparticles have the same characteristic peaks of Fe_3O_4 . This means that the crystal structure is not modified during the synthesis process, but the peak at $2\theta = 18.43^\circ$ that corresponds to (1 1 1) can be attributed to the existence of amorphous SiO_2 [35].

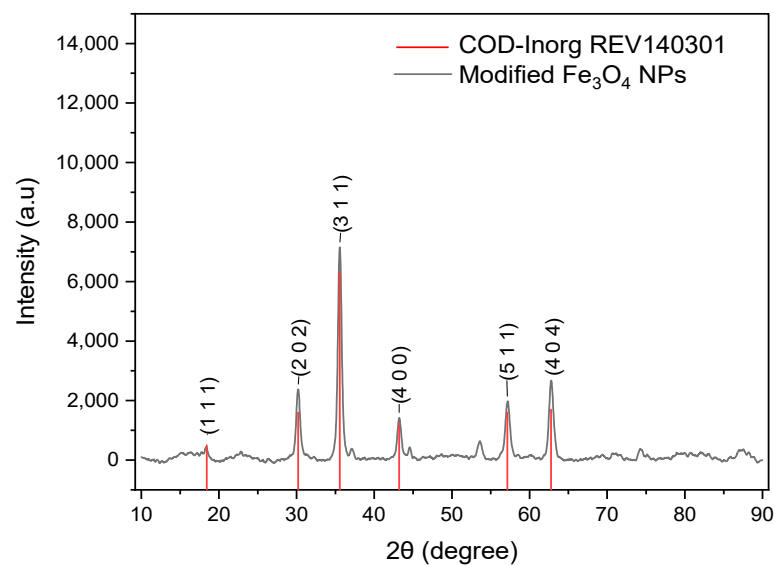


Figure 10. XRD patterns of modified Fe_3O_4 NPs.

With Match, the FWHM values were obtained in conjunction with the Scherrer equation. Crystal size was calculated in Table 5, where an average of 13.5 nm was obtained, which was greater than that of other authors [35] who obtained sizes of 7.6 nm, and it was inferior to the results in [33]. The authors calculated the crystal with the Scherrer equation and obtained sizes ranging from 80 to 108 nm, indicating that they used ultrasonic treatment and co-precipitation methods to synthesize $\text{Fe}_3\text{O}_4@\text{SiO}_2$. This smaller size of modified nanoparticle crystals can be attributed to the fact that the crystals were treated by ultrasound, which reduces particle size, increasing the surface area to which the enzyme adheres by covalent bonds [40].

Table 5. Calculated crystallographic parameters of modified Fe_3O_4 NPs with data obtained from XRD analysis using the Scherrer equation.

2θ (Degree)	(Hkl)	θ (Radian)	FWHM (Degree)	FWHM B (Radian)	Crystal Size D (nm)	Dislocation Density δ	Stress ε	Average Crystal Size D(nm)	Crystal Size De- viation D (nm)
18.43	(1 1 1)	0.1608	1.6281	0.0284	4.9433	0.0409	0.0438	13.5007	4.5466
30.19	(2 0 2)	0.2635	0.6828	0.0119	12.0507	0.0069	0.0110		
35.55	(3 1 1)	0.3102	0.5252	0.0092	15.8845	0.0040	0.0071		
43.22	(4 0 0)	0.3772	0.5777	0.0101	14.7912	0.0046	0.0064		
57.16	(5 1 1)	0.4988	0.5252	0.0092	17.2251	0.0034	0.0042		
62.78	(4 0 4)	0.5479	0.5777	0.0101	16.1093	0.0039	0.0041		

The difference between particle size measurement obtained in XDR and SEM analyses is due to distinct experimental conditions and measurement variations between each analysis. The agglomeration of nanoparticles, which can be observed in the micrographs obtained from SEM micrographs, does not allow for having an accurate measurement of the free and modified nanoparticles; however, the determination of both analyses is very valuable for knowing the structural and morphological properties and to verify the nanometric scale [28,41,42].

In Figure 11, the 451 cm^{-1} corresponds to that of the modified nanoparticles; this peak has a slight variation due to the modification process, so its location varies slightly and is characteristic of the tetrahedral and octahedral positions of iron [43,44]. The peak at

1062 cm^{-1} corresponds to the band of the silicon composition, which can be assigned to the stretching modes of the siloxane structure $\equiv\text{Si-O-Si}\equiv$ [43,44]. The peak at 1560 cm^{-1} (C-N vibrations) reflects that the APTMS is a similar compound to that in this work and only changes its orientation with the functional groups [39].

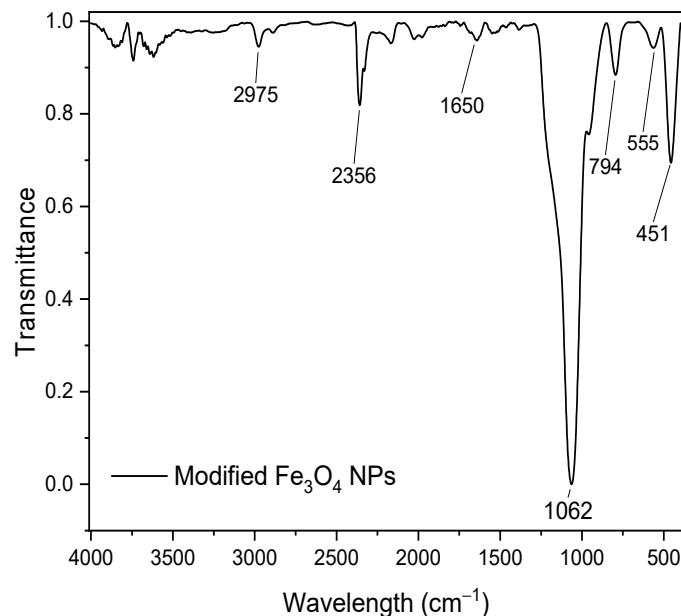


Figure 11. FTIR patterns of modified Fe_3O_4 NPs.

3.4. Immobilization of Modified Fe_3O_4 NPs ($\text{Fe}_3\text{O}_4@\text{SiO}_2\text{-PEI-Dextranase}$)

We observed an immobilization efficiency of 28.08%. Compared to other authors, this is lower. The authors of [23] reported a 72.38% immobilization efficiency, and other authors have reported an immobilization efficiency of 15.6% (w/w) of dextranase using the Epoxy CIM[®] Disk [25]. This result can be attributed to using a commercial enzyme; producing and purifying a pure enzyme is more advantageous than a commercial one. It was probably due to conformational and steric effects during the immobilization [25]. The fact that at one of the washing stages, a previous remnant reagent may have remained and again performed the process of obtaining nanoparticles could rule out these biases, and the use of a higher power magnet could improve the separation of the products.

As observed, the 24.375 mg/g is lower than 217.2 mg/g [23]. This can be attributed to the washing stage; some remnant reagents could have been left in previous stages, so that the complete activation of the functional groups around the enzyme was not carried out, which caused a decrease in sites where it could bind covalently to the PEI and thereby reduce the binding capacity of dextranase to nanoparticles.

3.5. Enzymatic Degradation of Dextran in Fermented Mash

Degradation kinetics were carried out in triplicate to observe the degradation behavior of free and immobilized enzymes; an initial concentration of 1935.90 ppm of dextran was observed. In Table 6, the removal presented in each experiment is observed.

Table 6. Residual dextran, residual DNS, and residual carbohydrate concentration after enzymatic degradation treatment with free enzyme and immobilized dextranase with Fe_3O_4 NPs.

Experiment	Enzyme	Temperature ($^{\circ}\text{C}$)	Time (h)	DNS(g/L)	Carbohydrates (g/L)	Dextran (ppm)	Removal %
1	Free	55	1	11.91 ± 0.11	14.89 ± 0.17	1647.60 ± 15.28	14.89
2	Free	55	2	9.38 ± 0.06	14.25 ± 0.09	752.25 ± 18.47	61.14
3	Nano	55	1	11.54 ± 0.18	14.43 ± 0.13	1329.30 ± 26.85	31.33
4	Nano	55	2	11.03 ± 0.09	15.59 ± 0.06	929.55 ± 20.74	51.98

Better removals have been obtained in less time [3] than the 60% removal at 35 °C for 4 h. It should be noted that the enzyme immobilization efficiency in the nanoparticles was 28%. Unless the immobilized enzyme obtained a slightly lower dextran removal than the free enzyme, it could be reused and easily separated using a magnet. On the other hand, PEI modification could have helped obtain a similar degradation performance, because it provides abundant amino groups to which dextranase would bind.

4. Conclusions

Sugarcane fermented mash contains sufficient fermentable sugars to be hydrolyzed by enzymatic degradation. Dextranase used for immobilization shows a wide range of thermal capabilities and stability at different pH levels that assure resistance in the harsh conditions of real industrial processes. The solvothermal process is elongated; however, it controls crystal size and shape. The obtained Fe₃O₄-modified NPs were spheres with an average size of 970 nm. SEM, EDS, FTIR, and XRD analysis showed Fe₃O₄ synthesis and the addition of a silica core shell in NPs. The calculated results with the Scherrer equation showed that ultrasonic treatment reduced average crystal size 6.6 times, providing a larger surface contact and more active sites to immobilize the enzyme. Even though Fe₃O₄@SiO₂-PEI-dextranase NPs had a 28% immobilization efficiency, they achieved a dextran degradation of 52%, close to the degradation percentage of the free enzyme (61%) for 2 h of hydrolysis of dextran. This could be considered a consequence of carrier modification with PEI that provides abundant functional amino groups to which enzyme proteins can bind and prevent particle agglomeration. The obtained immobilized enzyme (Fe₃O₄@SiO₂-PEI-dextranase) is a good option to degrade dextran in fermented mash. The immobilized enzyme can be easily recovered and recycled because of its magnetic properties. Therefore, dextranase-immobilized magnetic particles are expected to have potential applications in industrial fields.

Author Contributions: Conceptualization, D.C.-L.; Investigation, L.P.A.-G. and R.S.G.-P.; Methodology, L.P.A.-G. and D.C.-L.; Project administration, D.C.-L.; Supervision, G.L.S., G.R.U.-G. and D.C.-L.; Validation, G.L.S. and G.R.U.-G.; Writing—original draft, L.P.A.-G.; Writing—review and editing, L.P.A.-G. All authors have read and agreed to the published version of the manuscript.

Funding: This research received no external funding.

Institutional Review Board Statement: Not applicable.

Informed Consent Statement: Not applicable.

Data Availability Statement: Data is unavailable due to privacy or ethical restrictions.

Acknowledgments: The authors thank Tecnológico Nacional de México-TecNM for the support of the project with key 9981.1-P. The authors also thank CONACYT for the scholarships granted, with numbers 731921 and 759486. The authors thank Agileo Hernández-Gordillo and the Instituto De Investigación en Materiales, UNAM, Av. Universidad 3000, Copilco, C.P 04510, for their contribution to the characterization tests.

Conflicts of Interest: The authors declare no conflict of interest.

References

1. Abraham, K.; Hagen, S.; Schlumbach, K.; Rohde, A.; Flöter, E. Dextranase application in sucrose solutions-towards a better understanding. *Int. Sugar J.* **2016**, *118*, 582–588.
2. Bashari, M.; Touunkara, F.; Abdelhai, M.H.; Lagnika, C.; Xu, X.; Jin, Z. Impact of Dextranase on Sugar Manufacturing and its Kinetic on the Molecular Weights of Remaining Dextran. *Sugar Tech* **2013**, *15*, 84–93. [CrossRef]
3. Oropeza-De la Rosa, E.; López-ávila, L.G.; Luna-Solano, G.; Urrea-García, G.R.; Cantú-Lozano, D. Dextran hydrolysis and its rheology in mashes from bioethanol production process. *Rev. Mex. Ing. Quim.* **2019**, *18*, 543–554. [CrossRef]
4. Iqbal, S.; Marchetti, R.; Aman, A.; Silipo, A.; Qader, S.A.U.; Molinaro, A. Enzymatic and acidic degradation of high molecular weight dextran into low molecular weight and its characterizations using novel Diffusion-ordered NMR spectroscopy. *Int. J. Biol. Macromol.* **2017**, *103*, 744–750. [CrossRef] [PubMed]

5. Ding, Y.; Zhang, H.; Wang, X.; Zu, H.; Wang, C.; Dong, D.; Lyu, M.; Wang, S. Immobilization of Dextranase on Nano-Hydroxyapatite as a Recyclable Catalyst. *Materials* **2021**, *14*, 130. [\[CrossRef\]](#) [\[PubMed\]](#)
6. Kasaai, M.R. Dilute solution properties and degree of chain branching for dextran. *Carbohydr. Polym.* **2012**, *88*, 373–381. [\[CrossRef\]](#)
7. Zarour, K.; Llamas, M.G.; Prieto, A.; Rúas-Madiedo, P.; Dueñas, M.T.; de Palencia, P.F.; Aznar, R.; Kihal, M.; López, P. Rheology and bioactivity of high molecular weight dextrans synthesised by lactic acid bacteria. *Carbohydr. Polym.* **2017**, *174*, 646–657. [\[CrossRef\]](#)
8. Ninchan, B.; Vanichsriratana, W.; Sriroth, K. Investigation of the optimized dextran-degrading enzyme conditions on the decomposition of different molecular weights of pure dextran using response surface methodology. *Arch. Ind. Biotechnol.* **2016**, *1*, 8–19.
9. Bashari, M.; Jin, Z.; Wang, J.; Zhan, X. A novel technique to improve the biodegradation efficiency of dextranase enzyme using the synergistic effects of ultrasound combined with microwave shock. *Innov. Food Sci. Emerg. Technol.* **2016**, *35*, 125–132. [\[CrossRef\]](#)
10. Arabacı, N.; Karaytuğ, T.; Demirbas, A.; Ocsoy, I.; Kati, A. Nanomaterials for Enzyme Immobilization. In *Green Synthesis of Nanomaterials for Bioenergy Applications*; Wiley: Hoboken, NJ, USA, 2020; pp. 165–190. [\[CrossRef\]](#)
11. De Simone, A.; Naldi, M.; Bartolini, M.; Davani, L.; Andrisano, V. Immobilized Enzyme Reactors: An Overview of Applications in Drug Discovery from 2008 to 2018. *Chromatographia* **2019**, *82*, 425–441. [\[CrossRef\]](#)
12. Liu, D.M.; Chen, J.; Shi, Y.P. Advances on methods and easy separated support materials for enzymes immobilization. *TrAC—Trends Anal. Chem.* **2018**, *102*, 332–342. [\[CrossRef\]](#)
13. Bilal, M.; Zhao, Y.; Rasheed, T.; Iqbal, H.M.N. Magnetic nanoparticles as versatile carriers for enzymes immobilization: A review. *Int. J. Biol. Macromol.* **2018**, *120*, 2530–2544. [\[CrossRef\]](#) [\[PubMed\]](#)
14. Singh, M.; Ishfaq, N.; Salman, S.; Bashir, M.H.; Ashfaq, B. Enzyme Immobilization and Applications of Magnetic Nanoparticles in Smart Enzyme Immobilization. *Int. J. Res. Sci. Technol.* **2017**, *3*, 387–396.
15. Anwer, M.K.; Ali, E.A.; Iqbal, M.; Ahmed, M.M.; Aldawsari, M.F.; Saqr, A.A.; Ansari, M.N.; Aboudzadeh, M.A. Development of sustained release baricitinib loaded lipid-polymer hybrid nanoparticles with improved oral bioavailability. *Molecules* **2022**, *27*, 168. [\[CrossRef\]](#) [\[PubMed\]](#)
16. Lapitan, L.D.S.; Zhou, D. *A Simple Magnetic Nanoparticle-Poly-Enzyme Nanobead Sandwich Assay for Direct, Ultrasensitive DNA Detection*, 1st ed.; Elsevier Inc.: Amsterdam, The Netherlands, 2020; Volume 630, ISBN 9780128201435.
17. Gutarra, M.L.E.; Miranda, L.S.M.; De Souza, R.O.M.A. Enzyme Immobilization for Organic Synthesis. In *Organic Synthesis Using Biocatalysis*; Academic Press: Cambridge, MA, USA, 2016; pp. 99–126. [\[CrossRef\]](#)
18. Ansari, S.A.M.K.; Ficiara, E.; Ruffinatti, F.A.; Stura, I.; Argenziano, M.; Abollino, O.; Cavalli, R.; Guiot, C.; D’Agata, F. Magnetic iron oxide nanoparticles: Synthesis, characterization and functionalization for biomedical applications in the Central Nervous System. *Materials* **2019**, *12*, 465. [\[CrossRef\]](#) [\[PubMed\]](#)
19. Niculescu, A.G.; Chircov, C.; Grumezescu, A.M. Magnetite nanoparticles: Synthesis methods—A comparative review. *Methods* **2022**, *199*, 16–27. [\[CrossRef\]](#)
20. Shaikh, S.F.; Ubaidullah, M.; Mane, R.S.; Al-Enizi, A.M. *Types, Synthesis Methods and Applications of Ferrites*; Elsevier Inc.: Amsterdam, The Netherlands, 2020; ISBN 9780128192375.
21. Rao, B.G.; Mukherjee, D.; Reddy, B.M. *Novel Approaches for Preparation of Nanoparticles*; Elsevier Inc.: Amsterdam, The Netherlands, 2017; ISBN 9780323461481.
22. Alterary, S.S.; Alkhamees, A. Synthesis, surface modification, and characterization of Fe₃O₄@SiO₂core@shell nanostructure. *Green Process. Synth.* **2021**, *10*, 384–391. [\[CrossRef\]](#)
23. Wang, Y.; Wang, Q.; Song, X.; Cai, J. Improving the stability and reusability of dextranase by immobilization on polyethylenimine modified magnetic particles. *New J. Chem.* **2018**, *42*, 8391–8399. [\[CrossRef\]](#)
24. Prosheva, M.; Aboudzadeh, M.A.; Leal, G.P.; Gilev, J.B.; Tomovska, R. High-Performance UV Protective Waterborne Polymer Coatings Based on Hybrid Graphene/Carbon Nanotube Radicals Scavenging Filler. *Part. Part. Syst. Charact.* **2019**, *36*, 1800555. [\[CrossRef\]](#)
25. Bertrand, E.; Pierre, G.; Delattre, C.; Gardarin, C.; Bridiau, N.; Maugard, T.; Štrancar, A.; Michaud, P. Dextranase immobilization on epoxy CIM[®] disk for the production of isomaltooligosaccharides from dextran. *Carbohydr. Polym.* **2014**, *111*, 707–713. [\[CrossRef\]](#)
26. Gines-Palestino, R.S.; Oropeza-De la Rosa, E.; Montalvo-Romero, C. Cantú-Lozano Rheokinetic and effectiveness during the phenol removal in mescal vinasses with a rotary disk photocatalytic reactor (RDPR). *Rev. Mex. Ing. Química* **2020**, *19*, 653–665.
27. Deng, H.; Li, X.; Peng, Q.; Wang, X.; Chen, J.; Li, Y. Monodisperse magnetic single-crystal ferrite microspheres. *Angew. Chem. Int. Ed.* **2005**, *44*, 2782–2785. [\[CrossRef\]](#) [\[PubMed\]](#)
28. Manikandan, B.; Murali, K.R.; Rita, J. Optical, Morphological and Microstructural Investigation of TiO₂ nanoparticles for Photocatalytic application. *Iran. J. Catal.* **2021**, *3*, 1–11.
29. Oropeza-De la Rosa, E.; López-Ávila, L.G.; Luna-Solano, G.; Cantú-Lozano, D. Bioethanol production process rheology. *Ind. Crops Prod.* **2017**, *106*, 59–64. [\[CrossRef\]](#)
30. Palmonari, A.; Cavallini, D.; Sniffen, C.J.; Fernandes, L.; Holder, P.; Fagioli, L.; Fusaro, I.; Biagi, G.; Formigoni, A.; Mammi, L. Short communication: Characterization of molasses chemical composition. *J. Dairy Sci.* **2020**, *103*, 6244–6249. [\[CrossRef\]](#)
31. Ebaya, M.M.A.; El-Mowafy, M.; Adel El-Sokkary, M.M.; Hassan, R. Purification, Characterization, and Biocatalytic and Antibiofilm Activity of a Novel Dextranase from *Talaromyces* sp. *Int. J. Microbiol.* **2020**, *2020*, 9198048. [\[CrossRef\]](#)

32. Gibriel, A.Y.; Amin, A.A.; Nessrien Yassien, N.M.; El Banna, H.A.; Khaled, F.M. Characterization of Free and Immobilized *P. aculeatum* NRRL-896 Dextranase. *Int. J. Curr. Microbiol. Appl. Sci.* **2014**, *3*, 1135–1146.
33. Karimi Pasandideh, E.; Kakavandi, B.; Nasser, S.; Mahvi, A.H.; Nabizadeh, R.; Esrafil, A.; Rezaei Kalantary, R. Silica-coated magnetite nanoparticles core-shell spheres ($\text{Fe}_3\text{O}_4/\text{SiO}_2$) for natural organic matter removal. *J. Environ. Health Sci. Eng.* **2016**, *14*, 21. [\[CrossRef\]](#)
34. Mohammadi, H.; Nekobahr, E.; Akhtari, J.; Saeedi, M.; Akbari, J.; Fathi, F. Synthesis and characterization of magnetite nanoparticles by co-precipitation method coated with biocompatible compounds and evaluation of in-vitro cytotoxicity. *Toxicol. Rep.* **2021**, *8*, 331–336. [\[CrossRef\]](#)
35. Xu, J.; Ju, C.; Sheng, J.; Wang, F.; Zhang, Q.; Sun, G.; Sun, M. Synthesis and characterization of magnetic nanoparticles and its application in lipase immobilization. *Bull. Korean Chem. Soc.* **2013**, *34*, 2408–2412. [\[CrossRef\]](#)
36. Kayal, S.; Ramanujan, R.V. Doxorubicin loaded PVA coated iron oxide nanoparticles for targeted drug delivery. *Mater. Sci. Eng. C* **2010**, *30*, 484–490. [\[CrossRef\]](#)
37. Lesiak, B.; Rangam, N.; Jiricek, P.; Gordeev, I.; Tóth, J.; Kövér, L.; Mohai, M.; Borowicz, P. Surface Study of Fe_3O_4 Nanoparticles Functionalized With Biocompatible Adsorbed Molecules. *Front. Chem.* **2019**, *7*, 642. [\[CrossRef\]](#) [\[PubMed\]](#)
38. Nanditha, A.; Manokaran, J.; Balasubramanian, N. Fabrication of Lys-PVA- Fe_3O_4 modified electrode for the electrochemical determination of uric acid. *Res. J. Chem. Environ.* **2014**, *18*, 54–61.
39. Yang, L.; Tian, J.; Meng, J.; Zhao, R.; Li, C.; Ma, J.; Jin, T. Modification and characterization of Fe_3O_4 nanoparticles for use in adsorption of alkaloids. *Molecules* **2018**, *23*, 562. [\[CrossRef\]](#)
40. Lo, B.; Gorczyca, E.; Kasapis, S.; Zisu, B. Effect of low-frequency ultrasound on the particle size, solubility and surface charge of reconstituted sodium caseinate. *Ultrason. Sonochem.* **2019**, *58*, 104525. [\[CrossRef\]](#)
41. Aquino, P.; Osorio, A.M.; Ninán, E.; Torres, F. Characterization of ZnO nanoparticles synthesized by precipitation method and its evaluation in the incorporation in enamel paints. *Rev Soc Quím Perú.* **2018**, *84*, 17.
42. López-Cuenca, S.; Aguilar-Martínez, J.; Rabelero-Velasco, M.; Hernández-Ibarra, F.J.; López-Ureta, L.C.; Pedroza-Toscano, M.A. Spheroidal zinc oxide nanoparticles synthesized by semicontinuous precipitation method at low temperatures. *Rev. Mex. Ing. Química* **2019**, *18*, 1179–1187. [\[CrossRef\]](#)
43. Allafchian, A.R.; Jalali, S.A.H.; Amiri, R.; Shahabadi, S. Synthesis and characterization of the NiFe_2O_4 @TEOS-TPS@Ag nanocomposite and investigation of its antibacterial activity. *Appl. Surf. Sci.* **2016**, *385*, 506–514. [\[CrossRef\]](#)
44. Wencel, D.; Dolan, C.; Barczak, M.; Keyes, T.E.; McDonagh, C. Synthesis, tailoring and characterization of silica nanoparticles containing a highly stable ruthenium complex. *Nanotechnology* **2013**, *24*, 365705. [\[CrossRef\]](#)

Disclaimer/Publisher's Note: The statements, opinions and data contained in all publications are solely those of the individual author(s) and contributor(s) and not of MDPI and/or the editor(s). MDPI and/or the editor(s) disclaim responsibility for any injury to people or property resulting from any ideas, methods, instructions or products referred to in the content.